Optimal Scheduling of Wind Power Generators for Isolated Offshore Field Microgrids Considering Unified Frequency Response and Spinning Reserve

Jing Liu, Xiandong Xu, Longfei Liu, and Hongjie Jia, *Senior Member*, *IEEE*

***Abstract*—The high share of intermittent wind power jeopardizes system frequency security in isolated offshore field microgrids (IOFMs). Existing scheduling strategies, mainly focusing on stable energy supply and demand, fail to ensure frequency security due to the limited flexible and dispatchable resources in the IOFM. Thus, this paper proposes an optimal scheduling model of wind power generators with unified frequency response and spinning reserve constraints to assist operators in efficiently managing turbine generators. Frequency security indices are introduced to quantify the impact of both sudden wind power shortages and continuous wind power fluctuations on the frequency dynamics under different control modes. Based on these indices, unified frequency response and spinning reserve constraints are analytically derived to support the optimization of the control mode and on/off status of wind power generators. These highly nonlinear unified constraints are then reformulated as mixed-integer linear constraints, which are integrated into the scheduling model with operating costs as the objective. The proposed model is tested using a modified real-world IOFM. The results demonstrate that the proposed model not only ensures system frequency security but also reduces operating costs and carbon emissions.**

***Index Terms*—Frequency response, frequency security, microgrid, offshore oil and gas field, optimal scheduling, wind power, spinning reserve.**

I. Introduction

TO meet the escalating global energy demands while concurrently reducing carbon emissions, the pioneering integration of offshore wind power with traditional offshore oil and gas fields marks a significant shift in the energy sector [1]. As of now, notable projects in China and Norway underscore its viability [2]-[4]. However, the integration of wind power brings new challenges in the safe and economic operation.

Frequency stability is one of the operational challenges. Due to space and weight-bearing limitations, the rated capacity of gas/diesel turbine generators (TGs) is usually within the range of 1-10 MW with low rotational inertia. Significant frequency deviation occurs due to wind power fluctuations, which may lead to the tripping of wind turbines and TGs, as well as load shedding. These events pose a significant risk to the production safety of offshore oil and gas fields. The modelling of frequency dynamics within scheduling models is a relatively new research direction. The majority of studies focus on low-inertia bulk power systems, which can offer valuable insights for the isolated offshore field microgrid (IOFM).

Frequency security indices are the key factors to constructing frequency security constraints. Rate of change of frequency (RoCoF), frequency nadir, and quasi-steady-state frequency deviation are pivotal frequency security indices in the bulk power system [5], [6]. It is challenging to model frequency security indices due to the high complexity of frequency dynamics. By incorporating these indices, transient simulation and optimal scheduling are the two dominant methods for developing optimal operational strategies. Transient simulation evaluates the impact of wind power fluctuations on system frequency by simulating a multitude of operational scenarios and strategies [7]. Although this facilitates the derivation of secure operational strategies, it is resource-intensive and time-consuming. Consequently, the optimal scheduling attracts substantial attention. Notably, the frequency nadir exhibits significant nonlinearity. Incorporating the highly nonlinear frequency nadir constraint (FNC) poses a major challenge in its application.

To address this issue, several methods have been proposed to simplify the FNC, including constant parameter simplification model, reduced-order frequency response model, and machine learning techniques. In the method with the constant parameter simplification model, the rate of change in power disturbance and ramp rate of generators are simplified as constants [8], [9]. Despite its simplicity, this method cannot reflect the dynamics of the power-frequency response of generators, leading to an overestimation of the frequency regulation capability. Alternatively, methods with frequency response reduced-order models or machine learning techniques are developed to reformulate the linear FNC, offering a balance between computation feasibility and model fidelity. In the method with the reduced-order frequency response mod-

Manuscript received: August 24, 2024; revised: December 6, 2024; accepted: March 19, 2025. Date of CrossCheck: March 19, 2025. Date of online publication: April 5, 2025.

This work was supported in part by the project of National Key R&D Program of China (No. 2023YFC3106900) and the Science and Technology Program of China Southern Power Grid Co., Ltd. (No. GDKJXM20231008).

J. Liu, X. Xu (corresponding author), L. Liu, and H. Jia are with the School of Electrical and Information Engineering, Tianjin University, Tianjin 300072, China (e-mail: dmsliu@tju.edu.cn; xux27@tju.edu.cn; liudf307@foxmail.com; hjjia@tju.edu.cn).

DOI: 10.35833/MPCE.2024.000942

el [6], [10]-[12], a second-order model is derived to characterize the nonlinear FNC. Furthermore, the piece-wise linearization or convex hull estimation is used to transform the nonlinear FNCs into linear FNCs relevant to key parameters such as the droop coefficient, inertia constant, and fraction of total power from conventional generators. In [12], the governor model is further considered, but the dynamics of the prime mover are ignored. In [6], the consistent dynamics of the governors and prime movers of diesel generators as a generation group are taken into account. The criterion indicates that the frequency nadir is directly proportional to power disturbance magnitude. Nonetheless, the frequency nadir is still a nonlinear function regarding the parameters of governors and prime movers. To further improve the accuracy of the FNC model, machine learning techniques such as decision tree [13], deep neural network [14], [15], and extreme learning machine [16] are used to train the full-order frequency response model to estimate the frequency nadir. However, in comparison to methods based on the reduced-order model, machine learning techniques are susceptible to challenges in stability and robustness. These shortcomings stem from their limited interpretability, strong reliance on data quality and quantity, and uncertainty in generalization ability [17]. Such limitations may lead to the misidentification of unsafe operational areas, thereby posing a dramatic impact on the frequency stability.

The control mode employed by multiple TGs plays a key role in the frequency regulation, which makes it more difficult to quantify frequency security constraints. In the IOFM, the control mode for TGs with frequency response capacity includes droop speed control (usually represented directly by DROOP) mode and isochronous speed control (ISOCH) mode [18], [19]. The ISOCH mode is capable of automatically maintaining the system frequency at a set value. The DROOP mode can only achieve differential frequency adjustment and requires secondary adjustment to restore the system frequency to the set value. Among the aforementioned studies, only [6] and [12] are based on the ISOCH mode, while the others use the DROOP mode. This discrepancy underscores the need for further research tailored to the IOFM, particularly regarding the frequency regulation capability under different control modes.

Sufficient spinning reserves are indispensable for providing active power flexibility to support frequency regulation. The spinning reserve is vital in mitigating frequency deviations caused by wind power uncertainty. The difference in control parameters can lead to different allocation patterns of total spinning reserve among all online TGs when participating in frequency regulation. Existing studies on the spinning reserve in bulk power systems or microgrids are mostly based on statistical analysis of historical data [16], which faces critical limitations. On the one hand, the reliability of spinning reserve results may be jeopardized by the potential inadequacy or inaccuracy of historical data. On the other hand, it cannot reflect the distribution principle of spinning reserve among online TGs. Hence, it is necessary to quantify the total spinning reserve and clarify its distribution principle.

To fill the above gaps, an optimal scheduling model for TGs with unified frequency response and spinning reserve constraints is proposed for the IOFM. The main contributions are summarized as follows.

1) Two typical wind power disturbances are investigated to characterize the impact of wind power uncertainty on the frequency behaviors under normal and fault conditions. Novel frequency security indices are introduced to quantify frequency dynamics under different conditions and control modes. These indices could reflect the frequency security level and assist operators in monitoring frequency safety margins and the maximum wind power penetration level (MWPPL).

2) Existing DROOP-based frequency response and spinning reserve constraints for TGs are extended to incorporate fast regulation requirements for frequency response under various control modes. With the constraints, the proposed model could give optimal TG control mode, which plays a key role in supporting the integration of intermittent wind power.

3) An optimal spinning reserve allocation strategy under different control modes is proposed to ensure that all online TGs have sufficient spinning reserves for frequency regulation. This strategy would facilitate operators in determining the on/off status and control mode along with the variation of wind power penetration levels.

II. Operation Strategies of IOFM

Figure 1 shows a schematic diagram and operation strategy of IOFM. In the IOFM, multiple TGs (indexed by *tg*) and wind turbines supply power to the loads without relying on external grid support. As a result, the TGs and wind turbines need to be regulated frequently to maintain the balance of power supply and demand in the IOFM. The TGs in the IOFM can be operated in three control modes.

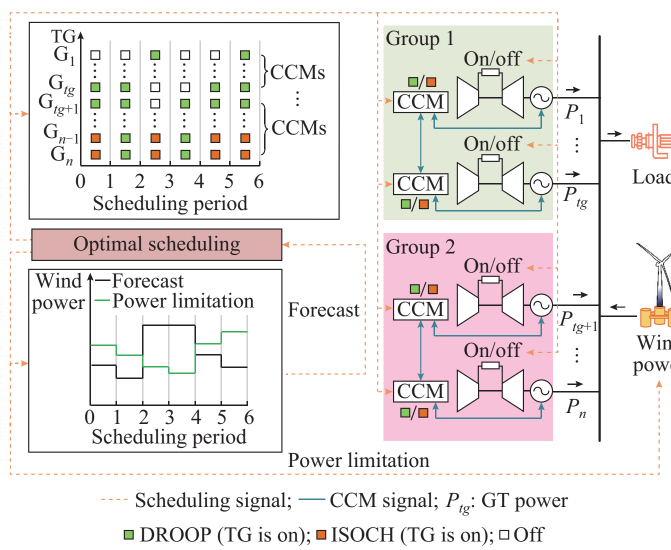

Fig. 1. A schematic diagram and operation strategy of IOFM.

1) Full isochronous control mode (FICM). TGs that are close to each other and equipped with compatible controllers are grouped together. TGs in different groups (e.g., group 1 and group 2) cannot cooperate with each other. Online TGs in either group 1 or group 2 operate in the ISOCH mode. Through the coordinative control of communication and control modules (CCMs), online TGs can operate stably at the

same load level [18]-[20]. Without CCMs, online TGs may interfere with each other during frequency regulation, which easily leads to system instability.

2) Full droop control mode (FDCM). All TGs operate in the DROOP mode, responding locally to wind power fluctuations based on system frequency. It can only achieve differential adjustment of system frequency. It is necessary to redistribute the load shared by TGs through the energy management system (EMS), so that online TGs can operate at the same load level and system frequency can be restored to the set value.

3) Hybrid control mode (HCM). Some online TGs in either group 1 or group 2 operate in the ISOCH mode, while the other TGs operate in the DROOP mode. When power fluctuations occur, all online TGs participate in frequency regulation. TGs in the ISOCH mode absorb all unbalanced power, while the power of TG in the DROOP mode returns to the initial setpoint. The EMS will periodically redistribute the power output setpoint of each TG and ensure that the TGs operate at the same load level.

To maximize wind power utilization while ensuring operation security, an operation strategy is proposed for TGs and wind turbines. An optimal scheduling model is proposed to implement the strategy. The on/off status and control mode of TGs are adjusted dynamically as wind power changes. And wind power operates in power-limited mode with power limitation signal from the proposed model. The model incorporates not only traditional steady-state operation constraints, but also frequency response and spinning reserves under different control modes, as shown in Fig. 1.

III. Unified Constraints for Frequency Response and Spinning Reserves

A. Frequency Security Indices Under Different Control Modes

This paper investigates the impact of wind power uncertainty on frequency safety under two typical operating conditions. Normal conditions examine the effects of continuous wind power fluctuations during normal operation. Fault conditions address the consequences of wind power tripping caused by accidents.

At present, the IOFM does not have strict requirements for RoCoF. Therefore, the frequency nadir and quasi-steady-state frequency deviation are regarded as frequency security indices to quantify the frequency characteristics of the IOFM. Corresponding to the two operating conditions, three frequency security indices are proposed, as shown in Fig. 2.

Assume that spinning reserves are sufficient regardless of the control mode in which online TGs operate. When disturbances occur at time t_1, the system frequency declines from its rated value f_0, as TGs operate in different modes including FDCM, FICM, and HCM. During wind power tripping, the system frequency undergoes a sharp drop. Conversely, when wind power fluctuates continuously, the system frequency changes more gradually. Specially, in Fig. 2(a), online TGs operate in the FDCM, which prevents automatic elimination of frequency deviation. Then, EMS redistributes power among the online TGs at time t_2, allowing the system frequency to progressively return to its rated value. In response to these disturbances, three indices are proposed to ensure the system frequency stability and protect the equipment security.

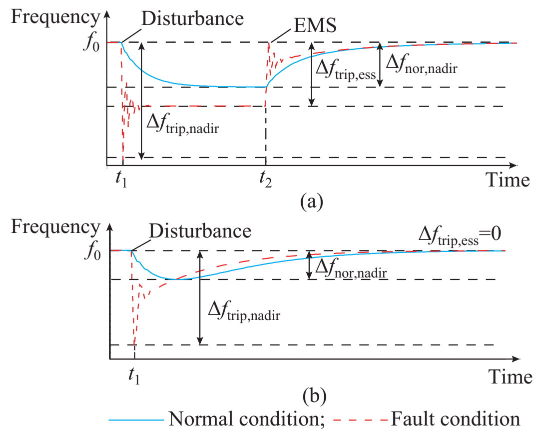

Fig. 2. Frequency security indices of IOFM under two operating conditions. (a) FDCM. (b) FICM or HCM.

1) $\Delta f_{\text{nor,nadir}}$ is the frequency nadir deviation under normal conditions (represented by NFND). Frequent wind power fluctuations may cause the frequency to frequently exceed the normal operating range, which affects its operation safety.

2) $\Delta f_{\text{trip,nadir}}$ is the frequency nadir deviation under fault conditions (represented by FFND), which is usually smaller than $\Delta f_{\text{nor,nadir}}$ in the IOFM. The sudden power loss caused by wind power tripping will lead to a rapid decrease in frequency. Exceeding a protection threshold will result in other generator trips or low-frequency load shedding, threatening the production safety.

3) $\Delta f_{\text{trip,ess}}$ is the quasi-steady-state frequency deviation under fault conditions (represented by FQSFD). The index is crucial for the IOFM to maintain stable operation until the EMS restores the system frequency to its set value. When FQSFD exceeds the acceptable threshold, it easily leads to system instability or potential equipment damage. Especially, since spinning reserves are sufficient when TGs operate in FICM or HCM, if there is a TG that operates in the ISOCH mode, $\Delta f_{\text{trip,ess}}=0$.

B. Aggregated Frequency Response Model Under Different Control Modes

The aggregated frequency response model under different control modes includes speed governor, prime mover, inertia and damping, and wind power, as shown in Fig. 3. Part of online TGs operate in the ISOCH mode. The others operate in the DROOP mode. In Fig. 3, s is the Laplace operator; $\Delta f(s)$ is the frequency deviation; $\Delta P_{\text{M}}(s)$ is the mechanical power variation of prime movers; $\Delta P_{\text{L}}(s)$ is the total load variation; $\Delta P_{\text{WT}}(s)$ is the wind power variation; H and D are the aggregated inertia time constant and damping coefficient, respectively; $T_{\text{t},tg}$ is the time constant of the prime mover; and $K_{\text{P},tg}$ and $K_{\text{I},tg}$ are the proportional and integral gains of the governor, respectively. Specially, $K_{\text{I},tg}=0$ represents the DROOP mode, and $K_{\text{I},tg}\neq 0$ represents the ISOCH mode.

According to the swing equation [16], the system frequency in the frequency domain is expressed as:

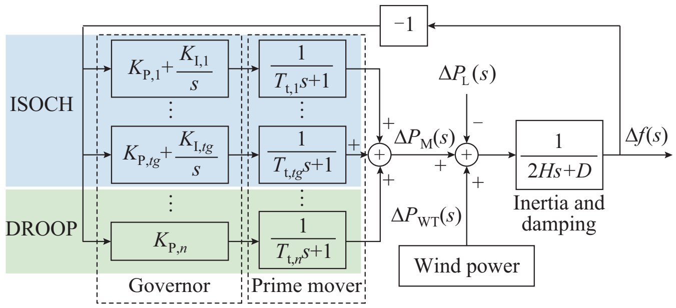

Fig. 3. Aggregated frequency response model in IOFM.

$$\Delta f(s)=\frac{\Delta P_{\mathrm{M}}(s)+\Delta P_{\mathrm{WT}}(s)-\Delta P_{\mathrm{L}}(s)}{2Hs+D} \tag{1a}$$

$$\Delta P_{\mathrm{M}}(s)=-\left(K_{\mathrm{P}}+\frac{K_{\mathrm{I}}}{s}\right)\frac{\Delta f(s)}{T_{\mathrm{t}}s+1} \tag{1b}$$

$$K_{\mathrm{I}}=\frac{1}{\sum\limits_{\forall tg}\mu_{tg}S_{\mathrm{N},tg}}\sum_{\forall tg}\mu_{tg}K_{\mathrm{I},tg}S_{\mathrm{N},tg} \tag{1c}$$

where T_{t} is the aggregated time constant of the prime mover; K_{P} and K_{I} are the aggregated proportional and integral gains of the governor, respectively; tg is the index of TGs in the IOFM, $tg\in\mathcal{G}$, and $\mathcal{G}$ is the set of TGs; μ_{tg} is the on/off status of TG tg; and $S_{\mathrm{N},tg}$ is the rated power capacity of TG tg. The derivations of H, T_{t}, and K_{P} can be found in [21] and [22].

The wind power model simulates continuous wind power fluctuations and sudden power shortages. Under normal conditions, the wind power variation is:

$$\Delta P_{\mathrm{WT}}(s)=-\frac{1}{T_{\mathrm{WT}}s+1}\frac{k_{\mathrm{WT}}\bar{P}_{\mathrm{WT}}}{s} \tag{2}$$

where k_{WT} is the fluctuation ratio of wind power; T_{WT} is the time constant of offshore wind power; and $\bar{P}_{\mathrm{WT}}$ is the maximum wind power that can be accommodated in the IOFM.

Under fault conditions, the wind power variation is:

$$\Delta P_{\mathrm{WT}}(s)=-\frac{\bar{P}_{\mathrm{WT}}}{s} \tag{3}$$

C. Frequency Response Constraints

Under normal conditions, the frequency response relevant to wind power fluctuations is expressed as:

$$\Delta F_{\mathrm{nor}}(s)=\Delta F_{\mathrm{nor,step}}(s)k_{\mathrm{WT}}\bar{P}_{\mathrm{WT}} \tag{4a}$$

$$\Delta F_{\mathrm{nor,step}}(s)=\frac{-1}{(2Hs^2+D_{\mathrm{eq}}s+K_{\mathrm{I}})(T_{\mathrm{WT}}s+1)} \tag{4b}$$

where $D_{\mathrm{eq}}=D+K_{\mathrm{P}}$. Due to $D\ll K_{\mathrm{P}}$, $D_{\mathrm{eq}}\approx K_{\mathrm{P}}$.

Under fault conditions, frequency response relevant to sudden power change is expressed as:

$$\Delta F_{\mathrm{trip}}(s)=\Delta F_{\mathrm{trip,step}}(s)\bar{P}_{\mathrm{WT}} \tag{5a}$$

$$\Delta F_{\mathrm{trip,step}}(s)=\frac{-s(T_{\mathrm{t}}s+1)}{2HT_{\mathrm{t}}s^3+(2H+DT_{\mathrm{t}})s^2+D_{\mathrm{eq}}s+K_{\mathrm{I}}}\frac{1}{s} \tag{5b}$$

In the IOFM, to automatically achieve the load-sharing at the same load level among online TGs, the speed governor controllers of online TGs are set with the same proportional gains. The load-sharing of TGs in the ISOCH mode is achieved with the help of real-time communication through CCMs [18]-[20]. In this way, it can be equivalent to the speed governor controllers of these TGs with the same integral gain.

Analytical expressions of the frequency response constraints are given by:

$$f_{\mathrm{nor}}(H,K_{\mathrm{I}})k_{\mathrm{WT}}\bar{P}_{\mathrm{WT}}\le\Delta\bar{f}_{\mathrm{nor,nadir}} \tag{6a}$$

$$f_{\mathrm{trip}}(H,K_{\mathrm{I}},T_{\mathrm{t}})\bar{P}_{\mathrm{WT}}\le\Delta\bar{f}_{\mathrm{trip,nadir}} \tag{6b}$$

$$\bar{P}_{\mathrm{WT}}\le zD_{\mathrm{eq}}\Delta\bar{f}_{\mathrm{trip,ess}}+(1-z)M_{\mathrm{big}} \tag{6c}$$

where $f_{\mathrm{nor}}(H,K_{\mathrm{I}})$ and $f_{\mathrm{trip}}(H,K_{\mathrm{I}},T_{\mathrm{t}})$ are the frequency nadir deviations of $\Delta F_{\mathrm{nor,step}}(s)$ and $\Delta F_{\mathrm{trip,step}}(s)$, respectively; z is an ancillary variable for different control modes of TGs, $z=1$ represents FDCM, and $z=0$ represents FICM or HCM; M_{big} is a constant coefficient and set as 10; $\Delta\bar{f}_{\mathrm{nor,nadir}}$ is the upper boundary of NFND; $\Delta\bar{f}_{\mathrm{trip,nadir}}$ is the upper boundary of FFND; and $\Delta\bar{f}_{\mathrm{trip,ess}}$ is the upper boundary of FQSFD.

D. Unified Spinning Reserve Constraints

The distribution of spinning reserves under different control modes are illustrated in Fig. 4. The spinning reserves vary under different control modes. When online TGs operate in either the FICM or the FDCM, spinning reserves are provided by all online TGs [18], [23], as depicted in Fig. 4(a) and (c), respectively. In contrast to Fig. 4(a) and (c), when online TGs operate in the HCM, spinning reserves are provided by the online TGs in the ISOCH mode, as shown in Fig. 4(b). Neglecting the influence of control modes on spinning reserve allocation may result in some TGs reaching their maximum power prematurely, preventing them from continuously participating in frequency regulation. Consequently, this reduction in available frequency regulation capacity can lead to increased frequency deviations.

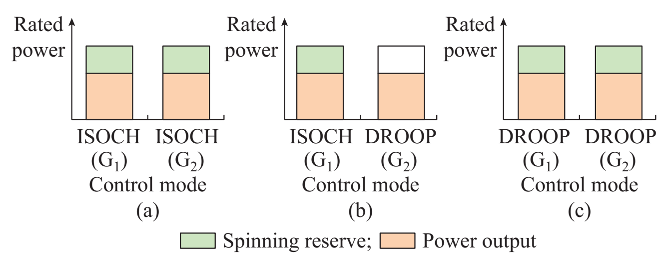

Fig. 4. Distribution of spinning reserves under different control modes. (a) FICM. (b) HCM. (c) FDCM.

The unified spinning reserve constraints for TGs are:

$$\mu_{tg}(\underline{P}_{tg}+x_{tg}P^{-}_{\mathrm{rev},tg})+\mu_{tg}zP^{-}_{\mathrm{rev},tg}\le P_{tg}\le$$
$$\mu_{tg}(\bar{P}_{tg}-x_{tg}P^{+}_{\mathrm{rev},tg})-\mu_{tg}zP^{+}_{\mathrm{rev},tg}\quad\forall tg \tag{7a}$$

$$x_{tg}\le x_{gr}\quad\forall tg\in\Omega_{gr},\forall gr \tag{7b}$$

$$\sum_{\forall tg\in\Omega_{gr}}x_{tg}\ge x_{gr}\quad\forall gr \tag{7c}$$

$$z=1-\sum_{\forall gr}x_{gr}\ge 0 \tag{7d}$$

where $P^{+}_{\mathrm{rev},tg}$ and $P^{-}_{\mathrm{rev},tg}$ are the upward and downward reserves of TG tg, respectively; x_{tg} is a binary variable that denotes the control mode of TG tg (when TG tg operates in the ISOCH mode, $x_{tg}=1$, and when TG tg operates in the DROOP mode, $x_{tg}=0$); gr is the index of TG groups in the IOFM in set $\mathcal{S}$ ($gr \in \mathcal{S}$); Ω_{gr} is the set of TGs in group gr, and $\bigcup_{\forall gr} \Omega_{gr} = \mathcal{G}$, $\Omega_{gr1} \cap \Omega_{gr2} = \varnothing$, $\forall gr1 \in \mathcal{S}$, $\forall gr2 \in \mathcal{S}$; and x_{gr} is a binary variable that indicates the operation state of group gr. When the TGs in group gr are allowed to operate in the ISOCH mode, $x_{gr}=1$; otherwise, $x_{gr}=0$. Formulas (7b)-(7d) indicate that there cannot be more than one group of TGs operating in the FICM or HCM. The TGs in other groups can only operate in the FDCM. When $z=1$, $x_{gr}=0, \forall gr$ and $x_{tg}=0, \forall tg$. In the FDCM, all online TGs operate in the DROOP mode, and the spinning reserves are shared by all online TGs simultaneously. When $z=0$, $\sum_{\forall gr} x_{gr} = 1$. There is only one group that has at least one TG operating in the ISOCH mode. And the total spinning reserve is borne by the TGs operating in the ISOCH mode.

The downward reserve to meet the total load fluctuations is:

$$\sum_{\forall tg} \mu_{tg}(x_{tg}+z_{sp})P^{-}_{\mathrm{rev},tg} \geq \beta^{-} \sum_{\forall pl} P_{pl} \tag{8}$$

where β^{-} is a constant for total loads and downward reserve; pl is the index of loads in the IOFM in set $\mathcal{L}$ ($pl \in \mathcal{L}$); and P_{pl} is the active power of load pl.

The upward reserve to meet the total load fluctuations and wind power uncertainty is:

$$\sum_{\forall tg} \mu_{tg} x_{tg} P^{+}_{\mathrm{rev},tg} \geq \beta^{+} \sum_{\forall pl} P_{pl} + \sum_{\forall wt} P_{wt} \tag{9}$$

where β^{+} is a constant related to total loads and upward reserve; and wind turbine wt belongs to the set of wind turbines $\mathcal{W}$ ($wt \in \mathcal{W}$).

IV. Optimal Scheduling Model with Unified Frequency Response and Spinning Reserve Constraints

A. Objective

Considering fuel and startup costs of TGs, carbon emission cost, and wind power cost, the objective function is:

$$\min\left(T\sum_{\forall sp}\sum_{\forall tg}\mu_{tg,sp}M_{tg,sp}c_{\mathrm{fuel},tg} + c_{\mathrm{WT}}T\sum_{\forall sp}\sum_{\forall wt}P_{wt,sp} + c_{\mathrm{CO2}}T\sum_{\forall sp}\sum_{\forall tg}\mu_{tg,sp}M_{tg,sp}m_{\mathrm{CO2},tg} + \sum_{\forall tg}\sum_{\forall sp}C_{\mathrm{on},tg,sp}\right) \tag{10}$$

where T is the time step of a scheduling period; $sp \in \mathcal{K}$, and $\mathcal{K}=\{1,2,...,N\}$ is the set of N scheduling periods; $M_{tg,sp}$ is the fuel consumption of TG tg during the sp^{th} scheduling period; $\mu_{tg,sp}$ is the on/off status of TG tg during the sp^{th} scheduling period; $c_{\mathrm{fuel},tg}$ is the unit cost of the fuel for TG tg during the sp^{th} scheduling period; c_{WT} is the unit cost of wind power; c_{CO2} is the unit cost of carbon emissions; $m_{\mathrm{CO2},tg}$ is the carbon emission of natural gas and crude oil per unit consumed by TG tg during the sp^{th} scheduling period; $P_{wt,sp}$ is the active power of wind turbine wt during the sp^{th} scheduling period; and $C_{\mathrm{on},tg,sp}$ is the start-up cost of TG tg during the sp^{th} scheduling period.

B. Operational Constraints

1) Offshore Wind Turbine

The operational constraints of wind turbines are expressed as:

$$0 \leq P_{wt,sp} \leq \bar{P}_{wt,sp} \quad \forall wt, \forall sp \tag{11a}$$

$$\underline{Q}_{wt} \leq Q_{wt,sp} \leq \bar{Q}_{wt} \quad \forall wt, \forall sp \tag{11b}$$

$$\underline{Q}_{wt,sp} = -P_{wt,sp}\tan(\arccos(\lambda_{\mathrm{lead},wt})) \quad \forall wt, \forall sp \tag{11c}$$

$$\bar{Q}_{wt,sp} = P_{wt,sp}\tan(\arccos(\lambda_{\mathrm{lag},wt})) \quad \forall wt, \forall sp \tag{11d}$$

$$\bar{P}_{\mathrm{WT},sp}S_{\mathrm{B},sp} - \sum_{\forall wt} P_{wt,sp} \geq 0 \quad \forall wt, \forall sp \tag{11e}$$

$$S_{\mathrm{B},sp} = \sum_{\forall tg}\mu_{tg,sp}S_{\mathrm{N},tg} \tag{11f}$$

where $P_{wt,sp}$ and $Q_{wt,sp}$ are the active power and reactive power of wind turbine wt during the sp^{th} scheduling period, respectively; $[\lambda_{\mathrm{lag},wt}, \lambda_{\mathrm{lead},wt}]$ are the power factor ranges of wind turbine wt; and $\overline{(\cdot)}$ and $\underline{(\cdot)}$ are the upper and lower boundaries of the variable, respectively. Formula (11e) indicates that the total active power of wind turbines cannot exceed the upper limit of wind power allowed to be accommodated by the IOFM during the sp^{th} scheduling period.

2) TG

The active and reactive power constraints and on/off constraints of TGs can be found in [10]. Load-sharing and fuel consumption constraints of TGs are given by [24]:

$$\mu_{tg,sp}\underline{\delta} \leq \frac{P_{tg,sp}}{\bar{P}_{tg}} \leq \mu_{tg,sp}\bar{\delta} \quad \forall tg, \forall sp \tag{12a}$$

$$\delta_{sp} + (\mu_{tg,sp}-1)\bar{\delta} \leq \frac{P_{tg,sp}}{\bar{P}_{tg}} \leq \delta_{sp} + (\mu_{tg,sp}-1)\underline{\delta} \quad \forall tg, \forall sp \tag{12b}$$

$$M_{tg,sp} = a_{tg}P_{tg,sp} + \mu_{tg,sp}b_{tg}P_{\mathrm{N},tg} \quad \forall tg, \forall sp \tag{12c}$$

where δ_{sp} is the load level of TGs during the sp^{th} scheduling period; a_{tg} and b_{tg} are the constant coefficients of the fuel-power characteristic equation; and $P_{\mathrm{N},tg}$ is the rated power of TG.

3) Power Flow Constraints

Due to the high charging capacitance and large line resistance to reactance ratio (R/X) of subsea cables, the active power and reactive power are closely coupled and related to the magnitude and phase angle of the bus voltage. Hence, power flow constraints are provided in [25].

4) Unified Frequency Response Constraints

Based on (6a)-(6c), the frequency response constraints in both ISOCH and DROOP are expressed as:

$$f_{\mathrm{nor}}(H_{sp}, K_{\mathrm{I},sp})k_{\mathrm{WT}}\bar{P}_{\mathrm{WT},sp} \leq \Delta\bar{f}_{\mathrm{nor,nadir}} \quad \forall sp \tag{13a}$$

$$f_{\mathrm{trip}}(H_{sp}, K_{\mathrm{I},sp}, T_{\mathrm{t},sp})\bar{P}_{\mathrm{WT},sp} \leq \Delta\bar{f}_{\mathrm{trip,nadir}} \quad \forall sp \tag{13b}$$

$$\bar{P}_{\mathrm{WT},sp} \leq \Delta\bar{f}_{\mathrm{trip,ess}}z_{sp}D_{\mathrm{eq}} + (1-z_{sp})M_{\mathrm{big}} \quad \forall sp \tag{13c}$$

$$H_{sp} = \frac{\sum_{\forall tg}\mu_{tg,sp}H_{tg}S_{\mathrm{N},tg}}{\sum_{\forall tg}\mu_{tg,sp}S_{\mathrm{N},tg}} \quad \forall sp \tag{13d}$$

$$K_{\mathrm{I},sp}=\frac{\sum_{\forall tg}\mu_{tg,sp}x_{tg,sp}K_{\mathrm{I},tg}S_{\mathrm{N},tg}}{\sum_{\forall tg}\mu_{tg,sp}S_{\mathrm{N},tg}}\quad \forall sp \tag{13e}$$

$$T_{\mathrm{t},sp}=\frac{\sum_{\forall tg}\mu_{tg,sp}T_{\mathrm{t},tg}S_{\mathrm{N},tg}}{\sum_{\forall tg}\mu_{tg,sp}S_{\mathrm{N},tg}}\quad \forall sp \tag{13f}$$

where H_{sp} is the aggregated inertia time constant during the sp^{th} scheduling period; $K_{\mathrm{I},sp}$ is the aggregated integral gain of the governor during the sp^{th} scheduling period; $T_{\mathrm{t},sp}$ is the aggregated time constant of the prime mover during the sp^{th} scheduling period; and $x_{tg,sp}$ is a binary variable that denotes the control mode of TG tg during the sp^{th} scheduling period.

5) Unified Spinning Reserve Constraints

The unified spinning reserve constraints in both ISOCH and DROOP are expressed as:

$$\sum_{\forall tg}\mu_{tg,sp}(x_{tg,sp}+z_{sp})P^{-}_{\mathrm{rev},tg,sp}\geq\beta^{-}\sum_{\forall pl}P_{pl,sp}\quad \forall sp \tag{14a}$$

$$\sum_{\forall tg}\mu_{tg,sp}x_{tg,sp}P^{+}_{\mathrm{rev},tg,sp}\geq\beta^{+}\sum_{\forall pl}P_{pl,sp}+\sum_{\forall wt}P_{wt,sp}\quad \forall sp \tag{14b}$$

$$\mu_{tg,sp}(\underline{P}_{tg}+x_{tg,sp}P^{-}_{\mathrm{rev},tg,sp})+\mu_{tg,sp}z_{sp}P^{-}_{\mathrm{rev},tg,sp}\leq P_{tg,sp}\leq \mu_{tg,sp}(\bar{P}_{tg}-x_{tg,sp}P^{+}_{\mathrm{rev},tg,sp})-\mu_{tg,sp}z_{sp}P^{+}_{\mathrm{rev},tg,sp}\quad \forall tg,\forall sp \tag{14c}$$

$$\mu_{tg,sp}\leq x_{gr,sp}\quad \forall tg\in\Omega_{gr},\forall gr,\forall sp \tag{14d}$$

$$\sum_{\forall tg\in\Omega_{gr}}x_{tg,sp}\geq x_{gr,sp}\quad \forall gr,\forall sp \tag{14e}$$

$$z_{sp}=1-\sum_{\forall gr}x_{gr,sp}\geq 0\quad \forall sp \tag{14f}$$

where $P^{+}_{\mathrm{rev},tg,sp}$ and $P^{-}_{\mathrm{rev},tg,sp}$ are the upward and downward reserves of TG tg during the sp^{th} scheduling period, respectively; and $x_{gr,sp}$ is a binary variable that indicates the operation state of group gr during the sp^{th} scheduling period.

C. Solution Method

The unified frequency response and spinning reserve constrained optimal model for the IOFM is:

$$\begin{cases}(10)\\ \text{s.t. } (11\text{a})\text{-}(14\text{f})\end{cases} \tag{15}$$

Nonlinear constraints such as (13a) and (13b) significantly increase the complexity of the optimization problem, thereby increasing its solution difficulty. Their transformation methods are as follows.

Formulas (13a) and (13b) are transformed into mixed-integer linear constraints by linearization techniques. By approximating the surface $f_{\mathrm{nor}}(H_{sp},K_{\mathrm{I},sp})$ with n_1 fitting planes, the linear constraints are expressed as:

$$f_{\mathrm{nor}}(H_{sp},K_{\mathrm{I},sp})\geq a_{i,0}+a_{i,1}K_{\mathrm{I},sp}+a_{i,2}H_{sp}\quad \forall i\in\{1,2,...,n_1\},\forall sp \tag{16}$$

where $a_{i,0}$, $a_{i,1}$, and $a_{i,2}$ are the coefficients of the i^{th} fitting plane of $f_{\mathrm{nor}}(H_{sp},K_{\mathrm{I},sp})$.

According to practices, $f_{\mathrm{trip}}(H_{sp},K_{\mathrm{I},sp},T_{\mathrm{t},sp})$ is less affected by $K_{\mathrm{I},sp}$, and can be approximated by $f_{\mathrm{trip}}(H_{sp},T_{\mathrm{t},sp})$. By approximating the surface $f_{\mathrm{trip}}(H_{sp},T_{\mathrm{t},sp})$ with n_2 fitting planes, the linear constraints are expressed as:

$$f_{\mathrm{trip}}(H_{sp},T_{\mathrm{t},sp})\geq b_{i,0}+b_{i,1}T_{\mathrm{t},sp}+b_{i,2}H_{sp}\quad \forall i\in\{1,2,...,n_2\},\forall sp \tag{17}$$

where $b_{i,0}$, $b_{i,1}$, and $b_{i,2}$ are the coefficients of the i^{th} fitting plane of $f_{\mathrm{trip}}(H_{sp},T_{\mathrm{t},sp})$.

Taking $f_{\mathrm{trip}}(H_{sp},T_{\mathrm{t},sp})$ as an example, the linearization method is described as follows. Firstly, the surface that consists of N_{p} discrete points is divided into N_{tri} triangular planes by the Delaunay triangulation. These planes form a set as $\phi=\{(a_{i,0},a_{i,1},a_{i,2})|a_{i,0}+a_{i,1}K_{\mathrm{I},sp,j}+a_{i,2}H_{sp,j}=0,\ j\in\mathcal{J}_i,\ i=1,2,...,N_{\mathrm{tri}}\}$. $\mathcal{J}_i$ is the set of the points in the i^{th} plane. Secondly, the K-means algorithm is used to cluster these planes in ϕ into n_1 clusters. And the clustering error is represented as $e=\sum_{i}^{n_1}\sum_{j\in\mathcal{C}_i}\left(\left|a_{i,0}+a_{i,1}K_{\mathrm{I},sp,j}+a_{i,2}H_{sp,j}-\hat{y}_j\right|/N_{\mathrm{p}}\right)$, where $\hat{y}_j$ is the real value when $j\in\mathcal{C}_i$; and $\mathcal{C}_i$ is the set of points in the i^{th} cluster. The method is validated in Supplementary Material A.

To eliminate the bilinear term $f_{\mathrm{nor}}(H_{sp},K_{\mathrm{I},sp})\bar{P}_{\mathrm{WT},sp}$, by assuming the maximum value of $\bar{P}_{\mathrm{WT},sp}$ as 1 and setting $\Delta f_{\mathrm{nor},sp}=f_{\mathrm{nor}}(H_{sp},K_{\mathrm{I},sp})$, the linear constraints of (13a) are given by [26]:

$$\frac{1}{2^K}\sum_{k=1}^{K}2^{k-1}v_{1,k,sp}\leq\Delta\bar{f}_{\mathrm{nor,nadir}}\quad \forall sp \tag{18a}$$

$$\Delta\underline{f}_{\mathrm{nor}}z_{1,k,sp}\leq v_{1,k,sp}\leq\Delta\bar{f}_{\mathrm{nor}}z_{1,k,sp}\quad \forall k,\forall sp \tag{18b}$$

$$\Delta\underline{f}_{\mathrm{nor}}(1-z_{1,k,sp})\leq\Delta f_{\mathrm{nor},sp}-v_{1,k,sp}\leq\Delta\bar{f}_{\mathrm{nor}}(1-z_{1,k,sp})\quad \forall k,\forall sp \tag{18c}$$

where $z_{1,k,sp}\in\{0,1\}$ and $v_{1,k,sp}$ are the ancillary variables, $k\in\{1,2,...,K\}$; and K is the number of piecewise linearization segments.

$f_{\mathrm{trip}}(H_{sp},K_{\mathrm{I},sp},T_{\mathrm{t},sp})$ is approximated by $f_{\mathrm{trip}}(H_{sp},T_{\mathrm{t},sp})$. To eliminate the bilinear term $f_{\mathrm{trip}}(H_{sp},T_{\mathrm{t},sp})\bar{P}_{\mathrm{WT},sp}$, by setting $\Delta f_{\mathrm{trip},sp}=f_{\mathrm{trip}}(H_{sp},T_{\mathrm{t},sp})$, the linear constraints of (13b) are [26]:

$$\frac{1}{2^K}\sum_{k=1}^{K}2^{k-1}v_{2,k,sp}\leq\Delta\bar{f}_{\mathrm{trip,nadir}} \tag{19a}$$

$$\Delta\underline{f}_{\mathrm{trip}}z_{2,k,sp}\leq v_{2,k,sp}\leq\Delta\bar{f}_{\mathrm{trip}}z_{2,k,sp}\quad \forall k,\forall sp \tag{19b}$$

$$\Delta\underline{f}_{\mathrm{trip}}(1-z_{2,k,sp})\leq\Delta f_{\mathrm{trip},sp}-v_{2,k,sp}\leq\Delta\bar{f}_{\mathrm{trip}}(1-z_{2,k,sp})\quad \forall k,\forall sp \tag{19c}$$

where $z_{2,k,sp}\in\{0,1\}$ and $v_{2,k,sp}$ are the ancillary variables.

The linear constraints of (13d) are given by [27]:

$$\sum_{\forall tg}z_{\mathrm{H},tg,sp}S_{\mathrm{N},tg,sp}=\sum_{\forall tg}\mu_{tg,sp}H_{tg,sp}S_{\mathrm{N},tg}\quad \forall sp \tag{20a}$$

$$\mu_{tg,sp}\underline{H}\leq z_{\mathrm{H},tg,sp}\leq\mu_{tg,sp}\bar{H}\quad \forall tg,\forall sp \tag{20b}$$

$$\underline{H}(1-\mu_{tg,sp})\leq H_{sp}-z_{\mathrm{H},tg,sp}\leq\bar{H}(1-\mu_{tg,sp})\quad \forall tg,\forall sp \tag{20c}$$

where $z_{\mathrm{H},tg,sp}$ is an ancillary variable.

The linear constraints of (13e) are given by [27]:

$$\sum_{\forall tg}z_{\mathrm{KI},tg,sp}S_{\mathrm{N},tg,sp}=\sum_{\forall tg}z_{\mathrm{X},tg,sp}K_{\mathrm{I},tg,sp}S_{\mathrm{N},tg}\quad \forall sp \tag{21a}$$

$$z_{\mathrm{X},tg,sp}\leq\mu_{tg,sp}\quad \forall tg,\forall sp \tag{21b}$$

$$z_{\mathrm{X},tg,sp}\leq x_{tg,sp}\quad \forall tg,\forall sp \tag{21c}$$

$$z_{\mathrm{X},tg,sp}\geq\mu_{tg,sp}+x_{tg,sp}-1\quad \forall tg,\forall sp \tag{21d}$$

$$\mu_{tg,sp}\underline{K}_{\mathrm{I}} \le z_{\mathrm{KI},tg,sp} \le \mu_{tg,sp}\bar{K}_{\mathrm{I}} \quad \forall tg, \forall sp \tag{21e}$$

$$\underline{K}_{\mathrm{I}}(1-\mu_{tg,sp}) \le K_{\mathrm{I},sp} - z_{\mathrm{KI},tg,sp} \le \bar{K}_{\mathrm{I}}(1-\mu_{tg,sp}) \quad \forall tg, \forall sp \tag{21f}$$

where $z_{\mathrm{X},tg,sp} \in \{0,1\}$ and $z_{\mathrm{KI},tg,sp}$ are the ancillary variables.

Linear constraints of (13f) are given by [27]:

$$\sum_{\forall tg} z_{\mathrm{T},tg,sp} S_{\mathrm{N},tg} = \sum_{\forall tg} \mu_{tg,sp} T_{\mathrm{t},\,tg,sp} S_{\mathrm{N},tg} \quad \forall sp \tag{22a}$$

$$\mu_{tg,sp}\underline{T}_{\mathrm{t}} \le z_{\mathrm{T},tg,sp} \le \mu_{tg,sp}\bar{T}_{\mathrm{t}} \quad \forall tg, \forall sp \tag{22b}$$

$$\underline{T}_{\mathrm{t}}(1-\mu_{tg,sp}) \le T_{\mathrm{t}} - z_{\mathrm{T},tg,sp} \le \bar{T}_{\mathrm{t}}(1-\mu_{tg,sp}) \quad \forall tg, \forall sp \tag{22c}$$

where $z_{\mathrm{T},tg,sp}$ is the ancillary variable.

Eventually, the proposed model is transformed into a mixed-integer convex constrained problem, which can be solved by commercial solvers such as GUROBI.

V. Case Study

A. System Description

As shown in Fig. 5, a case extracted from a real-world offshore oil and gas field in North China is used to test the proposed model. The IOFM consists of four offshore platforms. Platform A1 is close to platform A2, while platform B1 is similarly close to platform B2. Platforms A1 and B1 are interconnected via a 15 km subsea cable. There are nine TGs, a gas compressor, and two oil pumps. The active power of typical loads and wind power curves in the IOFM are shown in Fig. 6. Relevant parameters are illustrated in Supplementary Material A Table SAI.

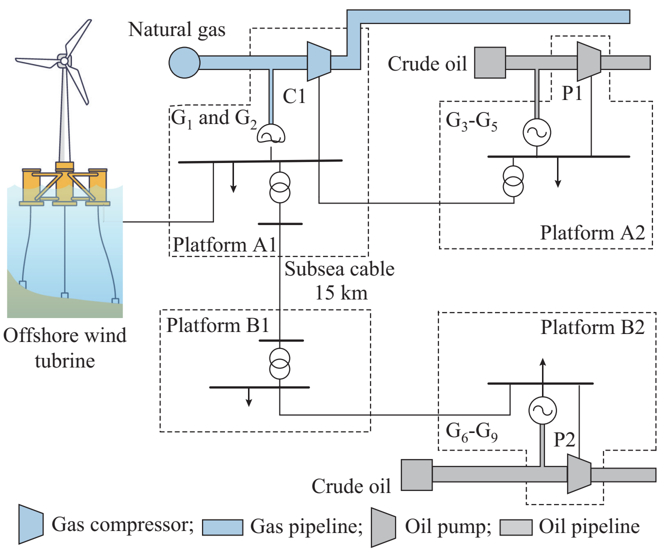

Fig. 5. System structure of IOFM.

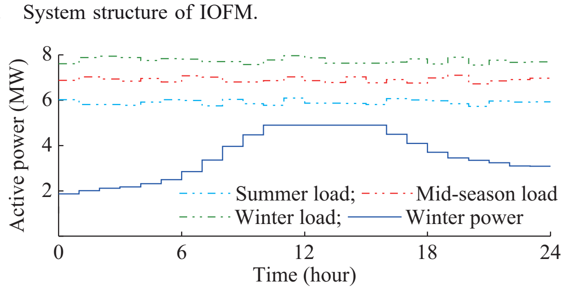

Fig. 6. Active power of typical loads and wind power curves in IOFM.

Four simulation scenarios are used to test the performance of the proposed model in Table I. Scenario 4 is used to simulate traditional IOFM without wind power. Compared with Scenario 4, Scenarios 1-3 are integrated with wind power to analyze the impact of wind power integration on the operation of IOFM. There are no frequency response constraints and coordinative control in Scenario 3. In Scenario 1, frequency response constraints are considered. No more than one TG can operate in the ISOCH mode. In Scenario 2, the coordinative control by CCMs is considered as well as frequency response constraints. All TGs are divided into three groups in Scenario 2, i.e., G1 and G2, G3-G5, and G6-G9. Only TGs in one group are allowed to operate in the ISOCH mode. TGs in other groups operate in the DROOP mode.

TABLE I
FOUR SIMULATION SCENARIOS

Scenario	Wind power	Frequency response constraints	Coordinative control
Scenario 1	√	√	×
Scenario 2	√	√	√
Scenario 3	√	×	×
Scenario 4	×	×	×

B. Result Analysis

1) Scheduling Results with Wind Power

Compared with Scenario 4, the reductions of operating cost and carbon emission, and the wind power utilization under different simulation scenarios and seasons are illustrated in Figs. 7 and 8, respectively.

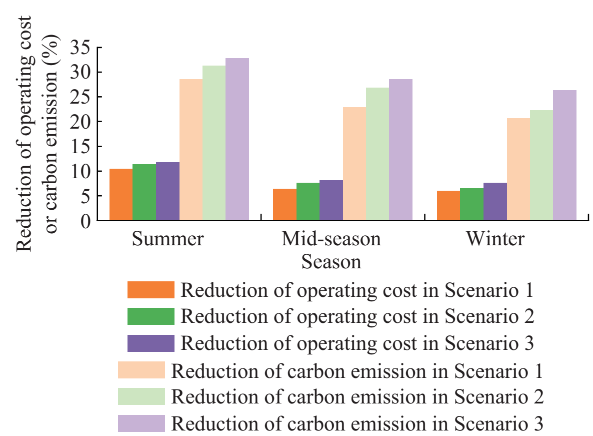

Fig. 7. Reductions of operating costs and carbon emissions under different simulation scenarios and seasons.

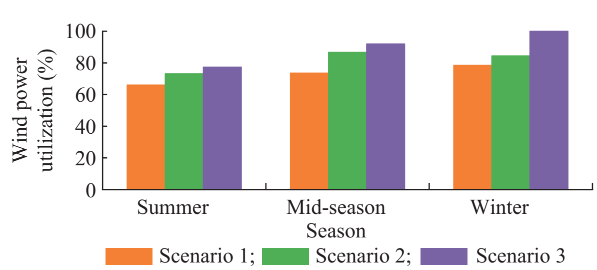

Fig. 8. Wind power utilization under different simulation scenarios and seasons.

Compared with Scenario 3, frequency response constraints are embedded in Scenarios 1 and 2. The reduction of operating cost in Scenario 1 decreases by 1.27%, 1.63%, and 1.61% in summer, mid-season, and winter in Fig. 7, respectively. In Scenario 2, it decreases by 0.38%, 0.47%, and 1.12%, respectively. Similarly, the reduction of carbon emission in Scenario 1 drops by 4.30%, 5.69%, and 5.64%, respectively.

In Scenario 2, it drops by 1.52%, 1.66%, and 4.07%, respectively. The wind power utilization is reduced by 11.26%, 18.37%, and 21.39% in Fig. 8, respectively. In Scenario 2, it is reduced by 4.15%, 5.37%, and 15.45%, respectively. The results indicate that frequency response constraints limit wind power utilization while ensuring system frequency safety.

Compared with Scenario 1, CCMs are further considered in Scenario 2 in addition to frequency response constraints. The reduction of operating cost in Scenario 2 is increased by 0.89%, 1.16%, and 0.49% in summer, mid-season, and winter, respectively. Carbon emission reduction is increased by 2.78%, 4.03%, and 1.57%, respectively. Wind power utilization is increased by 7.11%, 13.00%, and 5.94%, respectively. The reductions of operating cost and carbon emission, and wind power utilization in Scenario 2 are greater than those in Scenario 1, which is influenced by different control modes caused by CCMs.

2) Scheduling Wind Power and MWPPL

Wind power scheduling results under different scenarios and seasons are illustrated in Fig. 9. In summer, the maximum wind power in Scenarios 1 and 2 is 2.40 MW and 2.87 MW in Fig. 9(a), respectively. In mid-season, the maximum wind power in Scenarios 1 and 2 is 2.78 MW and 3.53 MW in Fig. 9(b), respectively. In winter, the maximum wind power in Scenarios 1 and 2 is 3.02 MW and 3.36 MW in Fig. 9(c), respectively. In different seasons, the wind power in Scenario 3 without frequency response constraints is no less than that in Scenarios 1 and 2 with frequency response constraints. In addition, the wind power in Scenario 2 is greater than that in Scenario 1, which is impacted by different control modes.

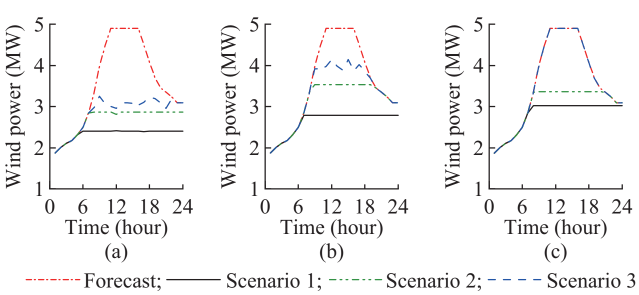

Fig. 9. Wind power scheduling results under different scenarios and seasons. (a) Summer. (b) Mid-season. (c) Winter.

The MWPPL under different scenarios and seasons is shown in Fig. 10. The MWPPL in Scenario 1 varies in different seasons. Similarly, the MWPPL in Scenarios 2 and 3 also varies. The MWPPL in Scenarios 1 and 2 is lower than that of Scenario 3 due to frequency response constraints. In summer, the MWPPL in Scenarios 1 and 2 is about 37% and 42%, respectively. In mid-season, the MWPPL in Scenarios 1 and 2 is about 41% and 32%, respectively. In winter, the MWPPL in Scenarios 1 and 2 is about 29% and 37%, respectively. Besides, MWPPL in Scenario 2 is greater than that in Scenario 1 due to the CCM. Hence, on the premise of ensuring frequency security, the frequency response constraints limit the MWPPL. Moreover, CCMs provide an effective method to improve the MWPPL.

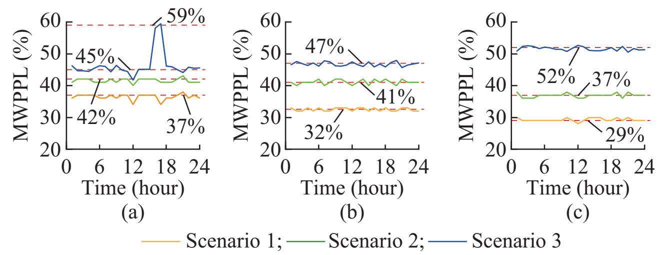

Fig. 10. MWPPL under different scenarios and seasons. (a) Summer. (b) Mid-season. (c) Winter.

3) Optimal Control Modes and On/off Status of TGs

The scheduling results of TGs during different seasons in Scenarios 1-3 are shown in Figs. 11-13, respectively. In Fig. 11(a), the TGs in Scenario 1 operate in the HCM during summer. The TG G1 adopts the ISOCH mode, while the other online TGs adopt the DROOP mode. In Fig. 11(b) and (c), all online TGs operate in the FDCM during mid-season and winter. In Fig. 12, the TGs in Scenario 2 operate in the HCM during different seasons. The TGs G1 and G2 adopt the ISOCH mode, while the other online TGs adopt the DROOP mode. In Fig. 13, the TGs in Scenario 2 operate in the FDCM during different seasons. The results indicate that the proposed model helps the system select the optimal on/off strategy and control mode for TGs.

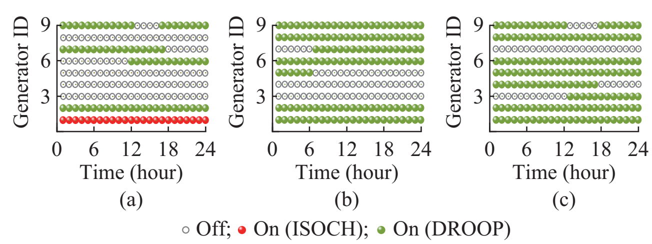

Fig. 11. Scheduling results of TGs during different seasons in Scenario 1. (a) Summer. (b) Mid-season. (c) Winter.

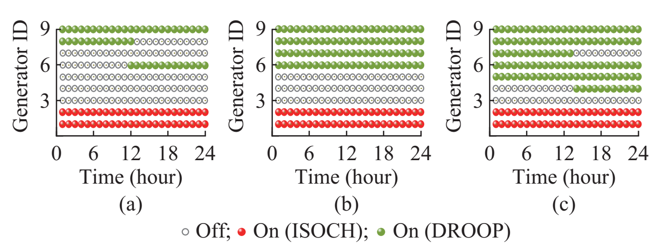

Fig. 12. Scheduling results of TGs during different seasons in Scenario 2. (a) Summer. (b) Mid-season. (c) Winter.

In addition, compared with Scenario 1, the reductions of operating cost and carbon emission, and wind power utilization in Scenario 2 in summer increase in Figs. 7 and 8. The results indicate that based on the CCM, the collaborative operation of multiple TGs under the ISOCH mode can effectively improve the system response to wind power fluctuations and enhance the consumption capacity of offshore wind power. Furthermore, although frequency response constraints limit the wind power utilization of the IOFM, the proposed model that accounts for TG control modes fully exploits the frequency regulation capacity of each TG, achieving the maximum wind power utilization while ensuring frequency safety.

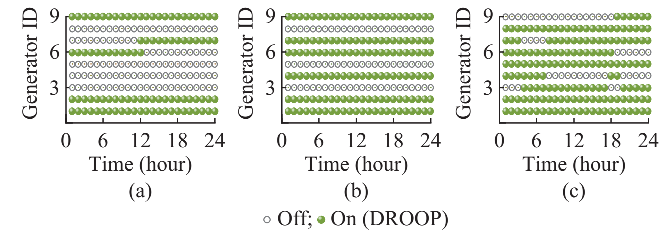

Fig. 13. Scheduling results of TGs during different seasons in Scenario 3. (a) Summer. (b) Mid-season. (c) Winter.

4) Spinning Reserve Allocation

The spinning reserves of TGs during different seasons in Scenarios 1-3 are depicted in Figs. 14-16, respectively.

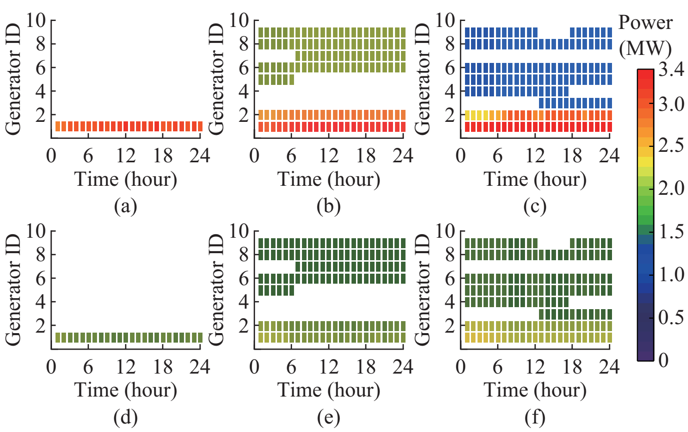

Fig. 14. Spinning reserve of TGs during different seasons in Scenario 1. (a) Upward reserve in summer. (b) Upward reserve in mid-season. (c) Upward reserve in winter. (d) Downward reserve in summer. (e) Downward reserve in mid-season. (f) Downward reserve in winter.

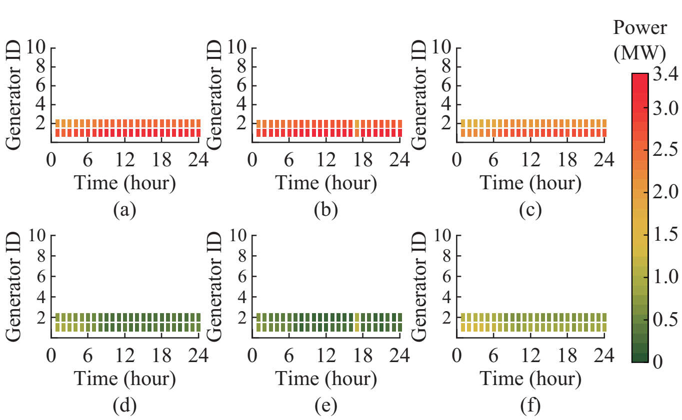

Fig. 15. Spinning reserve of TGs during different seasons in Scenario 2. (a) Upward reserve in summer. (b) Upward reserve in mid-season. (c) Upward reserve in winter. (d) Downward reserve in summer. (e) Downward reserve in mid-season. (f) Downward reserve in winter.

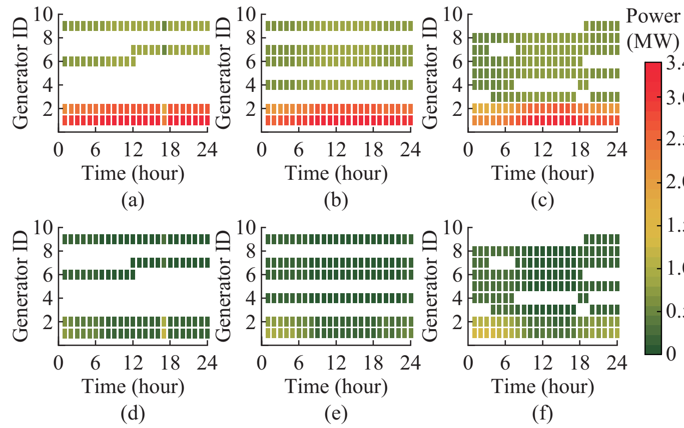

Fig. 16. Spinning reserve of TGs during different seasons in Scenario 3. (a) Upward reserve in summer. (b) Upward reserve in mid-season. (c) Upward reserve in winter. (d) Downward reserve in summer. (e) Downward reserve in mid-season. (f) Downward reserve in winter.

When online TGs operate in the HCM in Fig. 14(a) and Fig. 15, the spinning reserve is shared by the TGs in the ISOCH mode, because all unbalanced power resulting in frequency deviation is absorbed by TGs operating in the ISOCH mode to restore frequency at the set value. When online TGs operate in the FDCM as shown in Figs. 14(b), 14(c), and 16, the spinning reserve is shared by all online TGs at the same load level. In this mode, only part of the unbalanced power resulting in frequency deviation is absorbed by online TGs, because the FDCM cannot restore frequency at the set value.

VI. Conclusion

This paper proposes a unified frequency response and spinning reserve constrained scheduling model for wind power generators used in the IOFM, taking into account the switching of dynamic control modes. The conclusions are given as follows.

The proposed model realizes the optimal scheduling under different control modes while ensuring frequency security. With the introduction of coordinative control, the simultaneous operation of multiple TGs in ISOCH mode is achieved. Compared with the scenario without coordinative control, the operating costs are reduced by 0.89%, 1.16%, and 0.49%, and the MWPPL is enhanced by 5%, 9%, and 8% in summer, mid-season, and winter, respectively. In the scenario without coordinative control, the optimal control mode is HCM in summer, where only one TG operates in ISOCH mode, and FDCM in mid-season and winter. When the coordinative control is introduced, the optimal control mode in all seasons becomes HCM, which enables multiple TGs in one group to operate simultaneously in the ISOCH mode.

These findings underscore the crucial role of coordinative control among multiple TGs in minimizing the operating costs and wind power curtailment while ensuring frequency security in the IOFM. This also highlights the importance of selecting the control mode in wind power utilization.

Although this paper focuses on the IOFM, it can be adaptable to other isolated microgrids with appropriate modifications to some operational constraints. Potential applications include remote mining areas and industrial parks with integration of renewable energy.

In future works, more detailed theoretical analyses are required to investigate the relationship between unified frequency security and spinning reserve constraints, and the key parameters of TGs. And more advanced nonlinear optimization methods or hybrid methods will be conducted to further improve the precision of frequency security constraints without compromising computational efficiency. Additionally, the proposed model will be further extended to the IOFM with energy storage systems and flexible industrial demand response.

References

[1] M. Voldsund, A. Reyes-Lúa, C. Fu *et al*., "Low carbon power generation for offshore oil and gas production," *Energy Conversion and Management*, vol. 17, no. 1, p. 100347, Jan. 2023.

[2] Q. Wang, "Offshore wind power: an important opportunity for traditional oil and gas industry to realize low-carbon transformation," in *Annual Report on China's Petroleum, Gas and New Energy Industry*, 1st ed., Singapore: Springer Nature, Oct. 2022, pp. 231-245.

[3] A. van der Loos, H. E. Normann, J. Hanson *et al*., "The co-evolution of innovation systems and context: offshore wind in Norway and the Netherlands," *Renewable and Sustainable Energy Reviews*, vol. 138, p. 110513, Mar. 2021.

[4] CNOOC. (2023, May). CNOOC limited announces the world's first semi-submersible "double hundred" deep-sea floating wind turbine connected to the grid. [Online]. Available: https://www. cnoocltd. com/art/2023/5/20/art_55171_15338850.html

[5] B. Mohandes, M. S. El Moursi, N. Hatziargyriou *et al*., "A review of power system flexibility with high penetration of renewables," *IEEE Transactions on Power Systems*, vol. 34, no. 4, pp. 3140-3155, Jul. 2019.

[6] D. Lai, C. Chen, S. Tang *et al*., "Analytical derivation of frequency response rate constraint in distribution system restoration with single master diesel-based DG," *IEEE Transactions on Smart Grid*, vol. 14, no. 2, pp. 1341-1344, Mar. 2023.

[7] Y. Xu, C.-C. Liu, K. P. Schneider *et al*., "Microgrids for service restoration to critical load in a resilient distribution system," *IEEE Transactions on Smart Grid*, vol. 9, no. 1, pp. 426-437, Jan. 2018.

[8] F. Teng, V. Trovato, and G. Strbac, "Stochastic scheduling with inertia-dependent fast frequency response requirements," *IEEE Transactions on Power Systems*, vol. 31, no. 2, pp. 1557-1566, Mar. 2016.

[9] S. Han, M. He, Z. Zhao *et al*., "Overcoming the uncertainty and volatility of wind power: day-ahead scheduling of hydro-wind hybrid power generation system by coordinating power regulation and frequency response flexibility," *Applied Energy*, vol. 333, p. 120555, Mar. 2023.

[10] M. Paturet, U. Markvic, S. Delikaraoglou *et al*., "Stochastic unit commitment in low-inertia grids," *IEEE Transactions on Power Systems*, vol. 35, no. 5, pp. 3448-3458, Sept. 2020.

[11] Y. Shen, W. Wu, B. Wang *et al*., "Optimal allocation of virtual inertia and droop control for renewable energy in stochastic look-ahead power dispatch," *IEEE Transactions on Sustainable Energy*, vol. 14, no. 3, pp. 1881-1894, Jul. 2023.

[12] O. Bassey, K. L. Butler-Purry, and B. Chen, "Dynamic modeling of sequential service restoration in islanded single master microgrids," *IEEE Transactions on Power Systems*, vol. 35, no. 1, pp. 202-214, Jan. 2020.

[13] D. T. Lagos and N. D. Hatziargyriou, "Data-driven frequency dynamic unit commitment for island systems with high RES penetration," *IEEE Transactions on Power Systems*, vol. 36, no. 5, pp. 4699-4711, Sept. 2021.

[14] Y. Zhang, C. Cui, J. Liu *et al*., "Encoding frequency constraints in preventive unit commitment using deep learning with region-of-interest active sampling," *IEEE Transactions on Power Systems*, vol. 37, no. 3, pp. 1942-1955, May 2022.

[15] Y. Zhang, C. Chen, G. Liu *et al*., "Approximating trajectory constraints with machine learning-microgrid islanding with frequency constraints," *IEEE Transactions on Power Systems*, vol. 36, no. 2, pp. 1239-1249, Mar. 2021.

[16] L. Liu, Z. Hu, Y. Wen *et al*., "Modeling of frequency security constraints and quantification of frequency control reserve capacities for unit commitment," *IEEE Transactions on Power Systems*, vol. 39, no. 1, pp. 2080-2092, Jan. 2024.

[17] S. Zhong, K. Zhang, M. Bagheri *et al*., "Machine learning: new ideas and tools in environmental science and engineering," *Environmental Science & Technology*, vol. 55, no. 19, pp. 12741-12754, Aug. 2021

[18] M. Farrokhabadi, C. A. Canizares, and K. Bhattacharya, "Unit commitment for isolated microgrids considering frequency control," *IEEE Transactions on Smart Grid*, vol. 9, no. 4, pp. 3270-3280, Jul. 2018.

[19] M. Lambert and R. Hassani, "Diesel genset optimization in remote microgrids," *Applied Energy*, vol. 340, pp. 121036-121036, Jun. 2023.

[20] A. Bradley. (2014, Nov.). Combination generator control module catalog numbers 1407-CGCM user manual. [Online]. Available: https://literature. rockwellautomation. com/idc/groups/literature/documents/um/1407-um001_-en-p.pdf

[21] Q. Shi, F. Li, and H. Cui, "Analytical method to aggregate multi-machine SFR model with applications in power system dynamic studies," *IEEE Transactions on Power Systems*, vol. 33, no. 6, pp. 6355-6367, Nov. 2018.

[22] J. Li, Y. Qiao, Z. Lu *et al*., "Integrated frequency-constrained scheduling considering coordination of frequency regulation capabilities from multi-source converters," *Journal of Modern Power Systems and Clean Energy*, vol. 12, no. 1, pp. 261-274, Jan. 2024.

[23] J. Liu, L. Liu, X. Xu *et al*., "Improved load-sharing strategy for multiple turbine generators of offshore oil and gas fields with offshore wind power," *Sustainable Energy Technologies and Assessments*, vol. 73, p. 104092, Jan. 2025.

[24] H. G. Svendsen. (2022, Feb.). Optimised operation of low-emission offshore oil and gas platform integrated energy systems. [Online]. Available: https://arxiv.org/abs/2202.05072?context=eess

[25] Z. Yang, K. Xie, J. Yu *et al*., "A general formulation of linear power flow models: Basic theory and error analysis," *IEEE Transactions on Power Systems*, vol. 34, no. 2, pp. 1315-1324, Mar. 2019.

[26] W. Wu, Z. Tian, and B. Zhang, "An exact linearization method for OLTC of transformer in branch flow model," *IEEE Transactions on Power Systems*, vol. 32, no. 3, pp. 2475-2476, May 2017.

[27] H. Zhao. (2024, Feb.). Transformation techniques in optimization. [Online]. Available: https://hliangzhao.cn/materials/transformation-techs.pdf

Jing Liu received the B.S. degree from North China Electric Power University, Baoding, China, in 2017, and the M.S. degree from North China Electric Power University, Beijing, China, in 2020. He is currently pursuing the Ph.D. degree from Tianjin University, Tianjin, China. His research interests include modeling and optimal operation of offshore integrated energy system.

Xiandong Xu received the B.S. and Ph.D. degrees in electrical engineering from Tianjin University, Tianjin, China, in 2009 and 2015, respectively. He is an Associate Professor with Tianjin University, since 2020. His research interest includes flexibility of multi-energy system, particularly in industrial sector.

Longfei Liu received the B.S. degree from Tianjin University, Tianjin, China, in 2022. He is currently pursuing the M.S. degree from Tianjin University. His research interests include modeling and flexible control of offshore integrated energy system.

Hongjie Jia received the B.S., M.S., and Ph.D. degrees in electrical engineering from Tianjin University, Tianjin, China, in 1996, 1999, and 2001, respectively. He is currently a Professor with Tianjin University. His research interests include power reliability assessment, stability analysis and control, distribution network planning and automation, and integrated energy system.